Mineral and Geochemical Features of Sulfide in Jade Hydrothermal Field of Okinawa Trough

Yujie Wang and Zhigang Zeng *

Posted Date: 19 July 2023

doi: 10.20944/preprints202307.1255.v1

Keywords: Massive sulfide; Mineralization stage; Jade hydrothermal field; Okinawa Trough

Article

Mineral and Geochemical Features of Sulfide in Jade Hydrothermal Field of Okinawa Trough

Yujie Wang [1,2] and Zhigang Zeng [1,2,3,*]

[1] Seafloor Hydrothermal Activity Laboratory, CAS Key Laboratory of Marine Geology and Environment, Institute of Oceanology, Chinese Academy of Sciences, Qingdao 266071, China
[2] University of Chinese Academy of Sciences, Beijing 100049, China
[3] Laboratory for Marine Mineral Resources, Qingdao National Laboratory for Marine Science and Technology,Qingdao 266071, China
* Correspondence: Correspondence: zgzeng@ms.qdio.ac.cn

Abstract: In this phrase, mineralogical and elemental geochemical characteristics of massive sulfide samples collected from Jade hydrothermal field, located in the Izena depression in the central graben of Okinawa Trough, were analyzed by means of optical microscopy, scanning electron microscopy and electron probe. The results show that the sulfide in Jade hydrothermal area can be divided into Zn-Cu-Pb rich massive sulfide and Zn-Fe rich massive sulfide. The former is composed of sphalerite, galena, anglesite, chalcopyrite and pyrite, and its formation stage can be divided into pyrite stage, sphalerite-chalcopyrite stage, anglesite stage and colloform pyrite stage. The latter is mainly composed of sphalerite, pyrite, marcasite and a small amount of galena, which can be divided into galena stage, pyrite stage, sphalerite stage, pyrite and marcasite stage. Cu and Zn in pyrite may exist in the form of microinclusions, while Ag and Pb may exist in pyrite in the form of fine galena inclusions containing Ag. Fe and Cu may enter sphalerite in the form of ion replacement. Zn may enter chalcopyrite in the form of ion replacement. Consistent with the previous understanding, the metal elements in the hydrothermal liquid system in Jade hydrothermal field mostly migrate with the hydrothermal fluid as sulfur complexes, and when the hydrothermal fluid mixes with seawater, the physical and chemical conditions of the fluid change, resulting in sulfide mineral precipitation. However, the chemical structure of chalcopyrite is still controversial, which restricts the understanding of the substitution mechanism of trace elements during chalcopyrite precipitation.

Keywords: Massive sulfide; Mineralization stage; Jade hydrothermal field; Okinawa Trough

1. Introduction

The discovery of modern seafloor hydrothermal systems is one of the major events in the field of marine geological research in the 20th century [1]. They widely exist in extensional tectonic environments such as mid ocean ridges and backarc basins, as well as volcanic activity fields [2,3]. Driven by heat sources, seawater seeps down through crustal faults or cracks, transforms into hydrothermal fluids, and flows upward, forming hydrothermal products such as sulfides, hydrothermal columns, and metal bearing sediments at the vents. Its operation is accompanied by the interaction of seawater/fluid rock and/or sediment, the injection of magmatic materials, the mixing of seawater fluid, and the response and action of hydrothermal organisms, forming a large-scale massive accumulation of polymetallic sulfides. It not only has enormous economic value, but also has important research significance, and has become one of the major cutting-edge research fields in earth science today. By studying this natural laboratory, scientists can obtain information on the composition and temperature of hydrothermal fluids, and improve existing theories of hydrothermal mineralization [4]; In addition, comparative research with ancient continental massive sulfide deposits can also be conducted, providing theoretical guidance for exploring seafloor massive sulfide resources and laying a foundation for further understanding the hydrothermal mineralization process during the geological history [5].

 doi:10.20944/preprints202307.1255.v1

Previous systematic studies on mineralogy, geochemistry and isotopes have been carried out in the Okinawa Trough [6–14]. According to the existing geological and geophysical investigations, the Okinawa Trough is a back arc basin in the rift period, which is characterized by the development of brittle normal faults and frequent intrusion of magma, providing a favorable tectonic and magmatic environment for the development of hydrothermal systems [15]. Up to now, over 10 hydrothermal mineralization points have been discovered in the Okinawa Trough[16]. Among them, sulfide accumulations in Jade hydrothermal area are mainly composed of sphalerite (ZnS), wurtzite (ZnS), galena (PbS), anglesite($PbSO_4$), pyrite (FeS_2), marcasite (FeS_2), cubanite ($CuFe_2S_3$) and chalcopyrite ($CuFeS_2$). The average element composition of the whole rock samples of seafloor polymetallic sulfide is Zn (20.2%), Pb (11.8%), Ba (7.2%), Fe (6.2%), Cu (3.3%), As (17500 ppm), and Ag (2300 ppm) [17]. Nevertheless, further exploration is needed on important issues such as the mineral precipitation stage, chemical composition, and control factors of massive sulfides in the Jade hydrothermal field of the Okinawa Trough.

It is well known that the study of the mineral composition, fabric, mineral precipitation sequence[18,19] and geochemical characteristics [20,21] of hydrothermal sulfides can provide an important theoretical basis for further exploration of hydrothermal systems and mineralization through the indicator information of mineral genesis. Therefore, in this phrase, the structure, mineral assemblage and geochemical characteristics of sulfide samples collected from Jade hydrothermal area in the Okinawa Trough are studied. The controlling factors of mineral assemblage and geochemistry in hydrothermal sulfide of the Okinawa Trough and their reflection on hydrothermal activity characteristics are discussed.

2. Geologic Setting

The Okinawa Trough, located at the eastern margin of Eurasia, is a back arc basin formed by the NW subduction of the Philippine Sea plate under the Eurasian continental plate (Figure 1). At present, it is still in the early stage of back arc expansion [22,23], forming a complete trench arc basin system with the Ryukyu island arc and the Ryukyu trench. The Okinawa Trough is 230km wide in the north and 60-100km wide in the south, with water depth gradually increasing from north to south [22]. There have been reports of signs of oceanic crust appearing in its southern section [24], and the trough is intersected by a series of northwest trending strike slip faults, often divided into the northern, middle, and southern sections by the Tukara and Gonggu fault structural belts [25]. At the same time, the volcanic rocks exposed in the Okinawa Trough are mainly medium to acidic volcanic rocks, while basic basalts are rare. The rock types are mainly andesite, rhyolite, dacite, basalt and other calc alkaline series and tholeiite series [25,26]. In addition, due to the huge supply of terrestrial materials from the Yangtze and Yellow Rivers, the Okinawa Trough is covered with thick sediments, with the northern section covered by about 8km of sediments and the southern section covered by about 2km of sediments, which mainly composed of terrestrials and hydrothermal materials [23].

There is a diversity of sulfide and sulfate mineralization that can be explained by seafloor phase separation in the hydrothermal field of the Okinawa Trough, which is consistent with the shallow water depth of 700m-1600m in the hydrothermal field of the trough[16]. Among them, the Jade hydrothermal field is one of the largest mining areas in the Okinawa Trough[10], distributed on the northeast slope of the Izena depression in the central part of the trough (27°15′ N, 127°4.5′ E). The area is distributed in a southwest northeast direction with a width of about 600m and a length of 1800m, at a water depth of around 1200-1600m [27]. The strong structural deformation leads to rugged terrain and the distribution of small stepped faults. The Jade hydrothermal field exhibits both high-temperature (320 °C) and low-temperature (124 °C) hydrothermal activities, with irregular distribution of sulfide sulfate chimneys and mound shaped accumulations. Except for some chimneys that collapse, most chimneys can stand upright up to 5m. The main ore minerals in sulfide accumulations in Jade hydrothermal area are sphalerite, galena, pyrite, marcasite and chalcopyrite, as well as pyrrhotite ($Fe_{1-x}S$), tetrahedrite($Cu_{12}As_4S_{13}$), stibnite (Sb_2S_3), orpiment (As_2S_3) and other As and Sb rich minerals. Bismuthinite (Bi_2S_3), mimetite ($Pb_2Pb_3[AsO_4]_3Cl$) and natural metals are

Preprints (www.preprints.org) | NOT PEER-REVIEWED | Posted: 19 July 2023 doi:10.20944/preprints202307.1255.v1

occasionally seen. Gangue minerals are mainly barite ($BaSO_4$), plaster ($CaSO4 \cdot 2H2O$), anhydrite ($CaSO_4$) and amorphous silicon, and occasionally carbonate minerals, such as calcite ($CaCO_3$) [10].

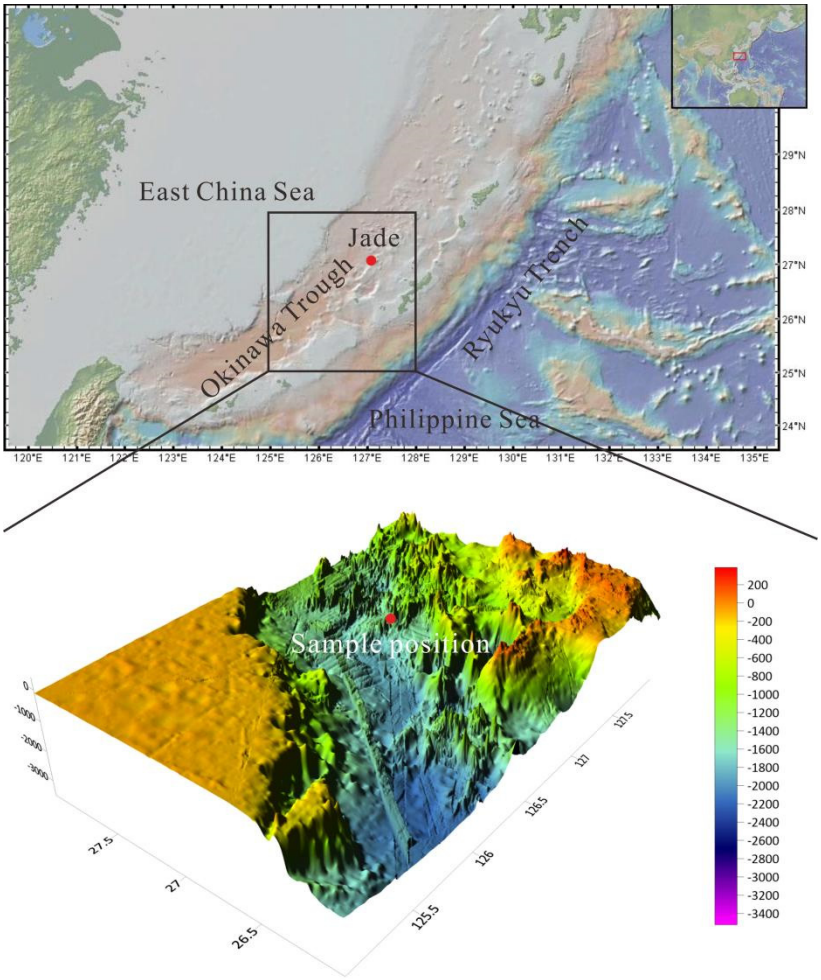

Figure 1. Locations of seafloor hydrothermal sulfide samples in the Jade hydrothermal field of the Okinawa Trough.

3. Material and Methods

The massive sulfide samples in this study were taken from the Jade hydrothermal area in the middle of the Okinawa Trough (Figure 1). They are mainly composed of sphalerite, barite, pyrite and chalcopyrite, containing a small amount of anglesite and galena, as well as a small amount of covellite, mimetite and crocoite ($PbCrO_4$). They are euhedral and subhedral grain structure, massive structure, and locally develop pore structure.

The thin sections of the samples was observed and identified in petrography and mineralogy with a polarizing microscope, and then the mineral composition of the samples was analyzed with a TESCAN VEGA 3LMH scanning electron microscope in the Key Laboratory of Marine Geology and Environment, Institute of Oceanology, Chinese Academy of Sciences. The electron microscope was equipped with a backscattered electron detector (BSE), a secondary electron detector and an Oxford INCA X-Max energy spectrometer (EDS), with an energy resolution of 124 eV (Mn Kα), Count rate>500000 cps, output rate>200000 cps. Analyze the samples at an accelerating voltage of 20 kV, an electron beam with a beam intensity of 15-798 pA, and a working distance of~15 mm. The resolution of the system is controlled by the beam spot size, and the beam spot size during analysis is 370 nm. BSE signals and EDS spectra are collected during the analysis. Use pyrite, sphalerite, galena, anorthite and quartz in the standard samples as the standard, and use XPP method to correct the results[28].

Preprints (www.preprints.org) | NOT PEER-REVIEWED | Posted: 19 July 2023 doi:10.20944/preprints202307.1255.v1

The JOEL JXA-8100 electron probe was used for major element analysis in the Analysis and Test Center of the Institute of Oceanology, Chinese Academy of Sciences. Analyses were conducted using an accelerating voltage of 15 kV and a beam current of 20 nA. Natural pyrite, sphalerite, galena and chalcopyrite were used for standardisation of Fe, Zn, Pb, Sb, Cu and S, while all other elements (Ni, As, Mo, Co and Ag) werestandardized on metals. Detection limits for S were ~74 ppm, for Mo ~205 ppm, for As ~137 ppm, for Fe ~218ppm, for Cu ~238 ppm, for Co ~117 ppm and for Zn ~223 ppm. Concentrations of Ag, Ni and Pb are generally around or below the minimum detection limit of the instrument (~145 ppm for Ag, ~133 ppm for Ni and ~393 ppm for Pb). After obtaining the experimental data, the Pearson correlation analysis of the elemental content was performed using SPSS.

4. Results

4.1. Mineralogical Characteristics

According to microscopic observation, the samples can be divided into rich Zn Fe massive sulfides (including HOK4, HOK41, and HOK42) and rich Zn Cu Pb massive sulfides (including HOK3, HOK31, and HOK 32). The Zn-Fe-rich massive sulfide samples are composed of sphalerite, pyrite and a small amount of galena. Galena is the first crystal, and is surrounded by sphalerite and pyrite (Figure 2f). Sphalerite is crystalline aggregate, coexists with pyrite, and is generally dendritic (Figure 2e). In general, the high-temperature hydrothermal environment is conducive to the slow growth of pyrite, and the crystal structure is more orderly. However, the crystallization of pyrite in low-temperature hydrothermal environment is accelerated, and more pyrite with lattice defects is produced [29]. Euhedral pyrite can be seen under the microscope, with single crystal output, which is presumed to be the product of early crystallization of hydrothermal activity. Some of the crystals are relatively intact, appearing as aggregates, and overall in bundles, branches, and chimneys. They undergo varying degrees of oxidation in the later stages, which is related to the exposure of the samples to the atmospheric environment. It can also be seen that pyrite is intertwined with marcasite, indicating that the physical and chemical conditions of the fluid have changed greatly in the later stage of the reaction, because marcasite is formed under the condition of pH<4.5 and the temperature is lower than 200 °C, while the stable state of pyrite is under the condition of pH>4.5 [18].

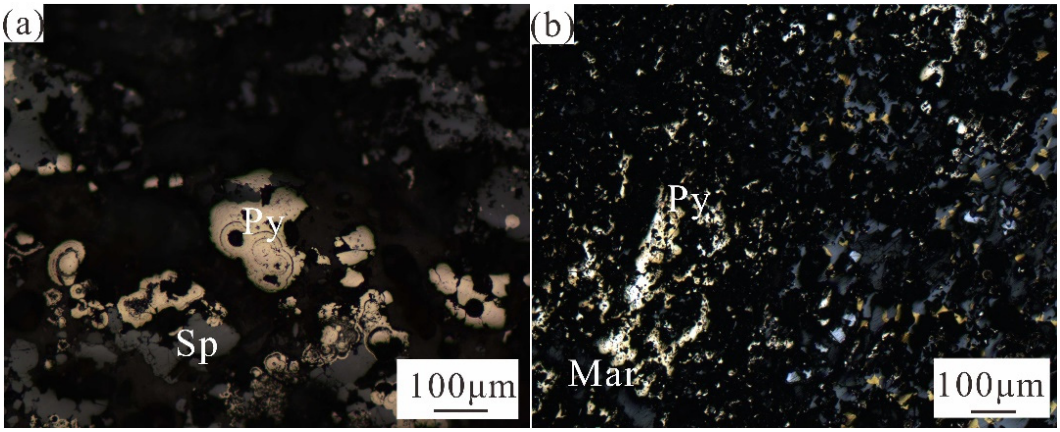

Preprints (www.preprints.org) | NOT PEER-REVIEWED | Posted: 19 July 2023 doi:10.20944/preprints202307.1255.v1

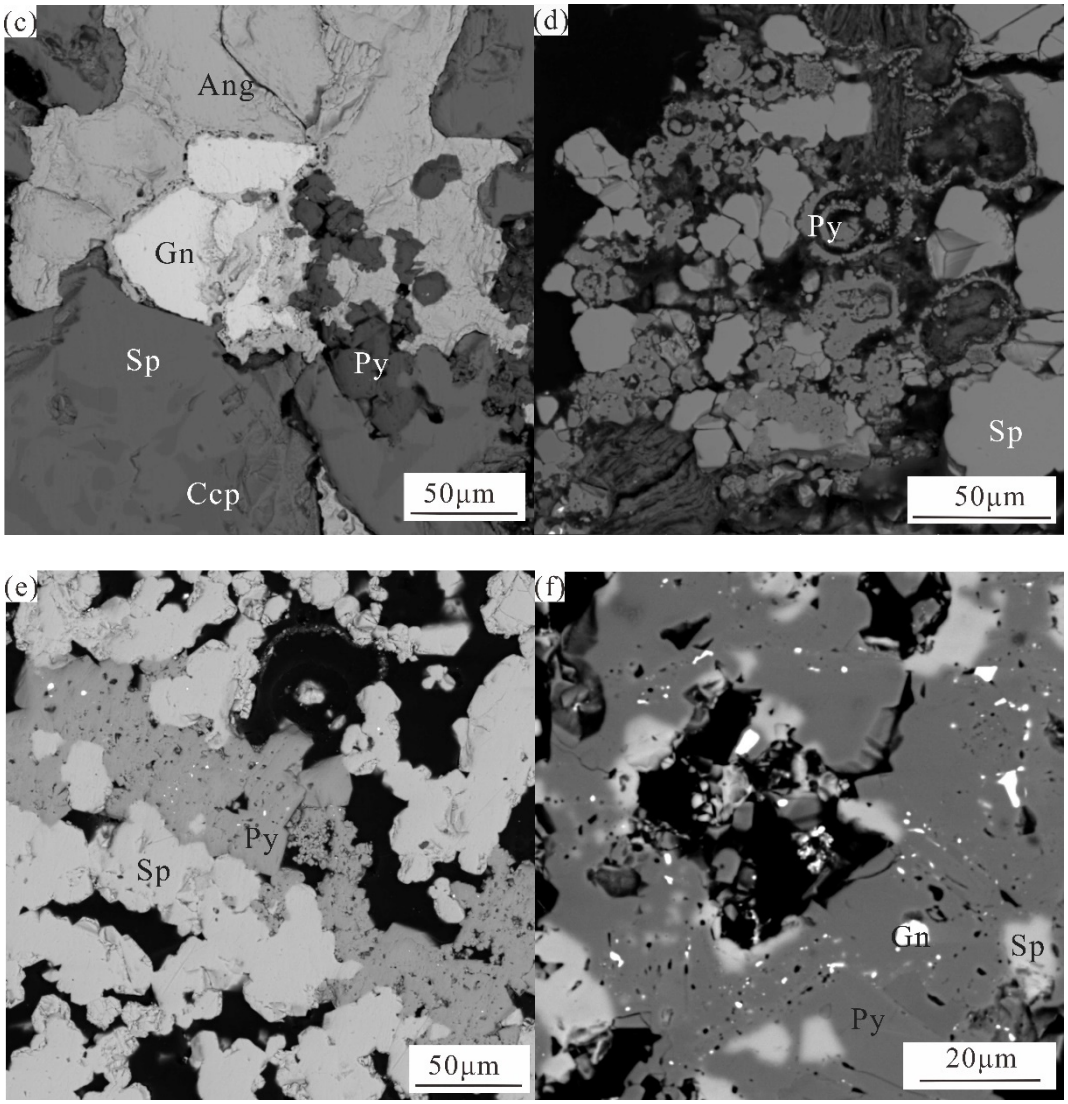

Figure 2. (**a**) colloform pyrite exists in the rim of sphalerite; (**b**) pyrite and marcasite are interwoven. Fine chalcopyrite scattered in sphalerite in the form of small spots; (**c**) fine pyrite surrounded by coarse sphalerite and anglesite, which may be formed by galena alteration; (**d**) colloform pyrite cements other sulfides. (**e**) Pyrite and sphalerite appear as aggregates, and overall in bundles, branches, and chimneys; (**f**) fine galena surrounded by pyrite.

Zn-Cu-Pb rich massive sphalerite is a mineral in the early stage of hydrothermal process, so it is mostly euhedral. Coarse grained sphalerite forms the overall framework of the ore, and part of it is cemented and interspersed along fractures by heteromorphic colloform pyrite formed later (Figure 2c). Chalcopyrite is scattered in sphalerite in the form of small spots or "milk drops", forming a "chalcopyrite virus" structure [17,30]. Since the contact boundary between chalcopyrite and sphalerite is smooth, no metasomatism or dissolution is found, it is speculated that chalcopyrite spots in sphalerite belong to exsolution origin. Anglesite is in square or irregular crystal shape, which encloses pyrite, sphalerite and other minerals precipitated earlier. It may be formed by galena alteration in late stage, so sporadic residual galena can be observed in anglesite (Figure 2c). Pyrite exists throughout hydrothermal mineralization and occurs in various forms. According to the mineral crystal morphology and the symbiotic association relationship between minerals, pyrite can be divided into several generations. The first generation is subhedral granular, which is surrounded by anglesite. The second generation of pyrite is formed into concentric ring ribbon and colloform due to the continuous leaching of hydrothermal fluid. Sulfide minerals generated in the early cementation

Preprints (www.preprints.org) | NOT PEER-REVIEWED | Posted: 19 July 2023 doi:10.20944/preprints202307.1255.v1

or exist in the particle gap of sphalerite crystal (Figure 2a), which is the product of the late hydrothermal activity, with local recrystallization (Figure 2d). Some pyrite and marcasite are interwoven (Figure 2b).

4.2. Chemical Characteristics

4.2.1. Pyrite

Pyrite is the most common mineral in hydrothermal activity. The electron probe point analysis (Table 1) of sulfide minerals in the samples shows that the average S/Fe atomic ratio of the three pyrite types is 1.99, 1.97 and 1.95, respectively, which are sulfur deficient. In the Zn-Cu-Pb-rich samples, the average value of S and Fe, the major element of colloform pyrite, is the smallest. Melekestseva et al.[31] found that the concentration of trace metals in massive pyrite has decreased compared with colloform pyrite, which is interpreted as the late pyrite crystallization is slow, so trace elements are easy to decompose into other sulfide phases rather than enter pyrite as solid solution. The content and distribution of trace elements are controlled by mineral type, mineral structure, zoning, and possible micro inclusions in individual minerals [32]. In most of pyrite, Zn is in the range of major elements (>1%), and Cu, Pb and As are in the range of minor elements (<0.1%) and trace elements (<0.01%) (Table 1).

4.2.2. Sphalerite

Sphalerite is the most dominant sulfide mineral in the samples. The electron probe results show that the main and trace element composition of sphalerite in Zn-Cu-Pb rich and Zn-Fe-rich samples is significantly different (Table 1). In the Zn-Cu-Pb-rich samples, the average Zn content of sphalerite is 63.493%, the average Cu content is 1.310%, and the average Fe content is 2.312%. Compared to this, the average content of Zn in the Zn-Fe-rich samples is relatively high, about 66.129%, while the Cu and Fe contents are relatively low, at 0.162% and 0.890%, respectively. The two have similar S content (33.620% and 33.653% respectively) and trace element content (such as As, Pb, Co, and Ni) (Table 1).

Table 1. Results of electron probe analysis of sulfide.

	Minerals		S(%)	Fe	Zn	Cu	Mo(ppm)	Ag	As	Pb	Co	Ni
Zn-Cu-Pb-rich massive sulfide	colloform pyrite	min	48.381	41.996	0.864	0.011	4220	160	140	—	110	—
		mean	50.465	44.481	1.457	0.310	4910	1080	6600	7230	470	30
		max	52.282	45.983	2.359	0.748	5500	3740	20020	42520	690	140
	Anhedral pyrite	min	49.155	41.448	0.109	—	4110	—	—	—	100	—
		mean	52.282	46.290	0.702	0.253	5190	160	2480	440	550	40
		max	54.621	47.913	3.354	6.043	5920	4240	28220	10930	900	350
	Sphaleri-te	min	31.747	0.718	49.543	—	2530	—	—	—	—	—
		mean	32.882	2.312	63.493	1.310	3420	—	60	90	40	40
		max	33.620	7.828	66.736	8.502	4050	—	420	1000	200	270
	Chalcopy-rite	min	33.217	27.421	0.133	30.696	2720	—	—	—	80	—
		mean	34.404	29.908	1.278	34.052	3470	130	40	40	310	40
		max	35.51	30.77	7.576	34.961	4020	580	260	510	610	160
Zn-Fe-rich massive sulfide	Anhedral pyrite	min	50.256	45.132	0.662	—	4480	—	—	—	430	—
		mean	51.544	46.090	1.155	0.161	5120	100	2710	40	590	50
		max	53.178	46.814	1.572	0.648	5870	420	23520	440	840	220
	Sphaleri-te	min	31.625	0.139	64.102	—	2450	—	—	—	—	—
		mean	32.740	0.890	66.129	0.162	3470	—	50	60	50	50
		max	33.653	1.949	67.404	1.075	4400	120	560	1350	360	370

4.2.3. Chalcopyrite

Chalcopyrite is a typical high-temperature mineral [33], of which its trace element characteristics are characterized by enrichment of Zn (0.133%-7.567%, average content 1.278%) and Mo (2720-4020 ppm, average content 3470 ppm), as well as trace amounts of Co (average content 310 ppm) and Ag (average content 130 ppm), and relatively low content of other trace elements (Table 1).

 doi:10.20944/preprints202307.1255.v1

5. Discussion

5.1. Seawater–Fluid Mixing and Element Enrichments

Research has shown that metal elements in hydrothermal fluids mainly migrate and transport in the form of complexes [34]. There are four main types of ligands in natural fluids: hydroxide, chloride, sulfate, and sulfide [35]. The study on the migration mechanism of metal elements in seafloor hydrothermal fluids shows that chlorine complexes and sulfur complexes are the two main forms of metal element migration in hydrothermal fluids, and the specific migration forms are closely related to the physical and chemical properties of the fluid. Chlorine complexes are important forms of metal element migration in high-temperature and high chloride fluids; Under relatively low temperature and low salinity conditions, sulfur complexes are the main form of metal element migration [36]. In addition, the mineralization temperature is often inevitably related to the mineralization stage, resulting in differences in the migration forms of metal elements in different hydrothermal activity stages [34].

Due to the lack of fluid information and the fact that the fluid inclusions in sulfide minerals are extremely small, their composition and temperature cannot be determined. Therefore, based on the mineral combinations of different stages, the sulfide deposits in the Jade hydrothermal region can be divided into two main mineralization stages. In the first mineralization stage of the formation of Fe-rich sulfide, due to the good crystal shape of pyrite, it can be considered that its mineralization temperature is relatively high, so some metal elements in this stage will be transported in the form of chlorine complexes, such as Fe and Cu. In the second mineralization stage, that is, the precipitation stage of Zn rich sulfide and colloform pyrite and other low temperature minerals, the metal elements should mostly migrate in the form of sulfur complexes.

A series of metal complexes with different migration forms in hydrothermal fluids can lose stability due to changes in the physical and chemical properties of the fluid, leading to precipitation. Thus, in the hydrothermal system of the Jade hydrothermal zone of the Okinawa Trough, metal elements mostly migrate in the form of sulfur complexes (the same as the 49.6°E hydrothermal zone of the Southwest Indian Ocean Ridge). When a large amount of hydrothermal fluid is mixed with seawater, the physical and chemical properties of the fluid change, and the H2S in the fluid decreases, the pH value increases, and the oxygen fugacity of the fluid increases, which in turn leads to the formation of sulfides in this field [35].

The trace element composition of pyrite can effectively reflect the composition and physicochemical properties (temperature, salinity, pH, sulfur fugacity, oxygen fugacity, etc.) of ore-forming fluid at different stages, so pyrite can be used as an indicator mineral of ore-forming fluid properties [37–39]. The research shows that the content of Co in pyrite is positively correlated with temperature [40], and the solubility of Mo drops sharply when the temperature is less than 350 °C [41], so the content of Mo in high-temperature sulfide is high [42]. It can be seen from the comparison that the Co (average content 470ppm) and Mo (average content 4910ppm) of colloform pyrite are the lowest (Table 1), so the hydrothermal temperature of colloform pyrite is the lowest when it is formed. In addition, the variation range of Co (430-840ppm) and Mo content (4480-5870ppm) of allomorphic pyrite rich in Zn-Fe-rich samples is smaller than that of allomorphic pyrite rich in Zn-Cu-Pb-rich samples (Table 1). It is speculated that pyrite in Zn- Fe-rich samples was formed in a more stable hydrothermal environment. The average contents of As (6600ppm), Ag (1080ppm) and Pb (7230ppm) in colloform pyrite are the highest (Table 1), and the possible existence forms of As in pyrite include substitution into pyrite lattice and micro inclusions [43] under low oxygen partial pressure and low temperature conditions [44,45], indicating that these elements tend to be enriched in hydrothermal sulfide at relatively low temperature[46]. Reith et al. [47] found that when the concentration of trace metals is only a few hundred ppm, it is likely to represent the solid solution in the pyrite lattice. In addition, the results of Vaughan and Rosso[48] show that Ni, Co, As and other trace elements usually exist in pyrite in the form of lattice replacement.

Fe^{2+}, Co^{2+} and Zn^{2+} have similar chemical properties, and are easy to enter sphalerite lattice in the form of divalent ions instead of Zn^{2+} [49]. The content of Fe in sphalerite can indicate the fluid

Preprints (www.preprints.org) | NOT PEER-REVIEWED | Posted: 19 July 2023 doi:10.20944/preprints202307.1255.v1

temperature when sphalerite is formed, which generally has a positive correlation relationship [50,51]. The content of Fe in sphalerite rich in Zn-Fe is low and its variation range is small, which indicates that the temperature of hydrothermal fluid is low when it is formed, and the fluctuation is small.

5.2. Element Correlation Analysis

Pyrite contains a large number of trace elements, including Cu, Zn, As, Ag, Pb, Co and Ni. Their occurrence forms in pyrite mainly include solid solution, nano invisible inclusion and micron visible inclusion [39,41,46]. Pearson correlation analysis of element content shows that Cu, Zn and Fe in pyrite are negatively correlated (Table 2). When the maximum value of Cu content in pyrite is 6.043%, the corresponding minimum value of Fe content is 41.448%. According to existing research, as copper loving elements, Cu and Zn are difficult to be isomorphic with Fe, and they often exist in the form of micro inclusions, such as extremely fine reticulated chalcopyrite [52]. Ag and Pb in pyrite are significantly positively correlated ($R_{Ag\text{-}Pb}$=0.402) (Table 2), which reflects the similar geochemical behavior of Ag and Pb in the process of mesothermal hydrothermal activity, or is the result of the leaching of early sulfide by later hydrothermal fluid, that is, element reactivation occurs at low temperature [53]. Generally, Pb is enriched in low-temperature minerals [54,55], and Ag and Pb may occur in pyrite in the form of fine galena inclusions containing Ag. As is a kind of metal element. Under the condition of reducing hydrothermal fluid, it mainly displaces S in pyrite [41,43,56]. Therefore, As in pyrite is negatively correlated with S ($R_{As\text{-}S}$=-0.456).

Table 2. Correlation matrix of some pyrite elements.

	S	Mo	Ag	As	Fe	Cu	Pb	Co	Zn
S	1								
Mo	0.170	1							
Ag	-0.207	0.043	1						
As	-0.456**	-0.175	0.202	1					
Fe	0.237	0.053	-0.374	-0.209	1				
Cu	-0.220*	0.042	0.060	0.047	-0.534**	1			
Pb	-0.155	-0.015	0.402	0.017	-0.435**	0.039	1		
Co	0.179	0.134	-0.058	0.015	0.278	-0.148	-0.095	1	
Zn	-0.227	-0.081	0.033	-0.069	-0.401*	-0.055	0.243	-0.219	1

The values followed by * are correlations at 95% confidence level**.** The values followed by ** are correlations at 99% confidence level.

Table 3. Correlation matrix of some sphalerite elements.

	S	Mo	Fe	Cu	Zn	As	Co
S	1						
Mo	-0.027	1					
Fe	0.115	0.000	1				
Cu	0.177	-0.038	.0833**	1			
Zn	-0.087	-0.024	-0.930**	-0.923**	1		
As	-0.012	0.016	0.030	-0.067	0.005	1	
Co	0.012	0.020	0.030	0.026	-0.036	-0.062	1

The values followed by * are correlations at 95% confidence level**.** The values followed by ** are correlations at 99% confidence level.

Preprints (www.preprints.org) | NOT PEER-REVIEWED | Posted: 19 July 2023 doi:10.20944/preprints202307.1255.v1

Table 4. Correlation matrix of some chalcopyrite elements.

	S	Mo	As	Fe	Cu	Co	Zn
S	1						
Mo	0.016	1					
As	0.334*	-0.271	1				
Fe	0.190	0.026	0.090	1			
Cu	0.087	-0.024	0.140	0.794**	1		
Co	0.065	0.092	0.033	0.021	-0.211	1	
Zn	-0.085	-0.100	-0.062	-0.827**	-0.778**	0.146	1

The values followed by * are correlations at 95% confidence level**.** The values followed by ** are correlations at 99% confidence level.

The change of trace elements in sphalerite can reach several orders of magnitude [40], which can indicate important geochemical information such as its formation environment. The content of Zn in sphalerite is significantly negatively correlated with that of Cu and Fe (R_{Zn-Cu}=-0.923; R_{Zn-Fe}=-0.930) (Table 3), and Cu and Fe are significantly positively correlated (R_{Fe-Cu}=0.833) (Table 3). Fe and Cu may enter sphalerite in the form of ion replacement. In addition, sphalerite in Zn-Cu-Pb-rich samples shows a "chalcopyrite virus" structure, so Cu may mainly exist in the inclusions formed by sphalerite cooling exsolution [32,57]. The content of Fe is an important indicator of the formation of sphalerite. Electron probe analysis shows that the content of Fe in sphalerite with "chalcopyrite virus" is significantly higher, and the content of Fe in cleaner sphalerite is lower, which may indicate the temperature difference between the two [51].

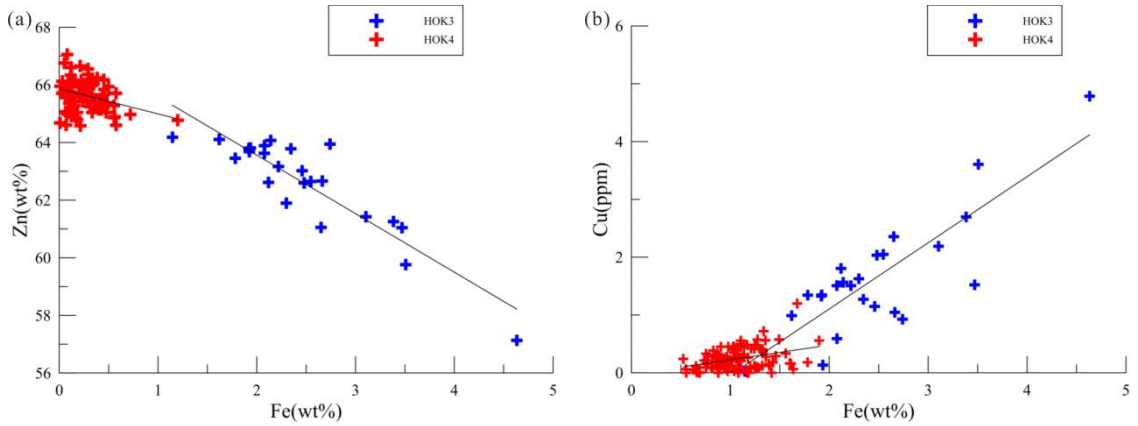

(**a**) (**b**)

Figure 3. (**a**) Correlation of Fe-Zn content in sphalerite. (**b**)Correlation of Fe-Cu content in sphalerite.

Zn in chalcopyrite is significantly negatively correlated with Cu and Fe contents (R_{Zn-Cu}=-0.778; R_{Zn-Fe}=-0.827) (Table 4). Zn enters chalcopyrite in the form of ion replacement potentially. As exists in chalcopyrite in the form of solid solution, and may also exist in the form of inclusion. At present, there is still a dispute about the chemical structure of chalcopyrite $Cu^{2+}Fe^{2+}S_2^{2-}$ [58,59], $Cu^{+}Fe^{3+}S_2^{2-}$ [60] or both [61], which restricts the understanding of the replacement mechanism of trace elements in chalcopyrite precipitation.

5.3. Mineral Precipitation Sequence and Growth Conditions

Multiple fluid inputs can form different types of sulfide symbiotic relationships and different distribution of trace elements. Changes in temperature and redox gradients of hydrothermal fluids can lead to changes in trace elements in different sulfides [62]. In the absence of in-situ hydrothermal fluid temperature data, the fluid conditions during mineral precipitation can be inferred based on mineral combinations, mineral morphology, and elemental chemical characteristics. For example, the mineral morphology of pyrite precipitated under different fluid conditions is different, euhedral and

 doi:10.20944/preprints202307.1255.v1

subhedral pyrite usually corresponds to higher fluid temperature and less fluid seawater mixing. colloform pyrite, on the other hand, shows a rapid and unbalanced crystallization process under the low temperature condition of seawater flooding [32,63]. The precipitation temperature of sphalerite is generally lower than 250 ℃[64,65]. The solubility of chalcopyrite in hydrothermal fluid below 350 ℃ drops sharply [66,67]. According to the temperature measurement formula of sphalerite: $Fe/Zn_{sphalerite}$=0.0013 (T) -0.2953[51]., the fluid temperature of Zn-Fe rich samples is about 229 ℃ - 250 ℃. The content of Fe and Zn in sphalerite of Zn-Cu-Pb-rich samples varies widely. It is calculated that the hydrothermal fluid temperature of sphalerite is about 235 ℃ - 271 ℃, reflecting the evolution process of hydrothermal activity temperature change.

It can be assumed that the mineral precipitation process follows the sequence of "high-temperature minerals precipitate first, low-temperature minerals precipitate later". According to the mineral precipitation sequence, the formation process of Zn-Cu-Pb rich massive sulfide can be divided into the following four stages: euhedral and subhedral pyrite crystallized in the early high-temperature hydrothermal fluid environment; Subsequently, the temperature of hydrothermal fluid decreased. So sphalerite precipitated at 235 ℃ - 271 ℃, accompanied by the dissolution of chalcopyrite. In the later stage, anglesite replace galena, and wrap pyrite and sphalerite formed in the early stage; Finally, colloform pyrite, the product of late hydrothermal activity, was precipitated at a lower hydrothermal fluid temperature. In Zn-Fe-rich samples, galena is an early crystalline mineral; The precipitation of minerals in the early stage led to the isolation of the rising hydrothermal fluid from the surrounding sea water, the increase of the temperature of the hydrothermal fluid, and the formation of euhedral and subhedral pyrite; Sphalerite crystallizes at a minimum temperature of 229 ℃ - 250 ℃, which is the result of moderate mixing of medium temperature, acidic, reducing hydrothermal fluid and seawater; With the turbulence of hydrothermal fluid conditions in the later period, pyrite and marcasite are interwoven. The formation of this sample underwent low high low fluid temperature conditions. In addition, because the chimney is "extinguished", the fluid temperature decreases, anhydrite is dissolved at low temperature or metasomatized by later sulfide [55,68], so there is no anhydrite in the sample.

6. Conclusion

The sulfides in the Jade hydrothermal area of the Okinawa Trough can be divided into Zn-Cu-Pb-rich massive sulfides and Zn-Fe-rich massive sulfides. In the Zn-Cu-Pb-rich massive sulfides, coarse-grained sphalerite forms the overall framework of the ore, and chalcopyrite is scattered in sphalerite in the form of tiny flecks or "milk drops", forming "chalcopyrite virus" structure. Minerals precipitated earlier are surrounded by anglesite, which may be formed by replacing galena. Pyrite exists throughout the hydrothermal mineralization and occurs in a variety of forms. In the Zn-Fe-rich massive sulfides, galena is the earliest to crystallize and is surrounded by sphalerite and pyrite. Sphalerite is less authigenic and coexists with pyrite, with an overall dendritic appearance. It can also be seen that pyrite and marcasite interweave and coexist.

The electron probe point analysis (Table 1) of sulfide minerals in the samples shows that the average S/Fe atomic ratio of the three pyrite types is 1.99, 1.97 and 1.95, respectively, which are sulfur deficient. In the Zn-Cu-Pb-rich samples, the average Zn content of sphalerite is 63.493%, the average Cu content is 1.310%, and the average Fe content is 2.312%. The average content of Zn in the Zn-Fe-rich samples is relatively high, about 66.129%, while the Cu and Fe contents are relatively low, at 0.162% and 0.890%, respectively. The trace element characteristics of chalcopyrite are characterized by enrichment of Zn (0.133%-7.567%, average content 1.278%) and Mo (2720 ppm-4020ppm, average content 3470ppm).

Colloform pyrite has the lowest Co and Mo content and the highest As, Ag and Pb content, indicating the lowest hydrothermal temperature at the time of colloform pyrite formation. The Zn-Fe-rich massive sulfides have a smaller range of variation in Co and Mo content in anhedral pyrite, which is speculated to form in a hydrothermal environment with more stable temperature. The negative correlation between Cu, Zn and Fe in pyrite suggests that these elements may be present as micro-inclusions, while the significant positive correlation between Ag and Pb in pyrite suggests that

Ag and Pb may be present in pyrite as fine Ag-bearing galena inclusions. The significant negative correlation of Zn with Cu and Fe in sphalerite suggests that Fe and Cu may have entered sphalerite as ion replacement. The significant negative correlation between Zn with Cu and Fe in chalcopyrite may indicate that Zn enters chalcopyrite in the form of ion replacement. The chemical structure of chalcopyrite is still controversial, which limits the understanding of the mechanism of trace element replacement during chalcopyrite precipitation.

The formation of Zn-Cu-Pb-rich massive sulfides is divided into the following four stages: euhedral-subhedral pyrite stage, sphalerite-chalcopyrite stage, anglesite stage and colloform pyrite stage. The formation of Zn-Fe-rich massive sulfides can be divided into galena stage, pyrite stage, sphalerite stage, and pyrite-marcasite stage.

Acknowledgments: We are grateful for the valuable comments and suggestions from the anonymous reviewers and editors. This work was supported by the National Natural Science Foundation of China (Grant Nos. 91958213, 42221005), Strategic Priority Research Program (B) of the Chinese Academy of Sciences (Grant No. XDB42020402), and Special Fund for the Taishan Scholar Program of Shandong Province (Grant No. ts201511061).

Reference

1. Parson, L.M.; L.M. Parson; C.L. Walker; D.R. Dixon; L. Geological Society of Hydrothermal vents and processes. *Geological Society special publication no. 87* **1995**, *1*, 1.
2. Alt, J.C., *Subseafloor processes in mid-ocean ridge hydrothermal systems*. 1995: Seafloor Hydrothermal Systems: Physical, Chemical, Biological, and Geological Interactions.
3. Tivey, M.K. Generation of Seafloor Hydrothermal Vent Fluids and Associated Mineral Deposits. *Oceanography* **2007**, *20*, 50-65.
4. Martin, A.J.; M. Keith; I. McDonald; K.M. Haase; K.A. McFall; R. Klemd; C.J. MacLeod Trace element systematics and ore-forming processes in mafic VMS deposits: Evidence from the Troodos ophiolite, Cyprus. *Ore Geology Reviews* **2019**, *106*, 205-225.
5. Pirajno, F. Hydrothermal processes associated with meteorite impact structures: evidence from three Australian examples and implications for economic resources. *Australian Journal of Earth Sciences* **2005**, *52*, 587-605.
6. Muehlenbachs, J. Hydrothermal sulfide and oxide deposits on seamounts near 21°N, East Pacific Rise. *GSA Bulletin* **1987**,
7. Halbach, P.; W. Hansmann; V. Koppel; B. Pracejus Whole-rock and sulfide lead-isotope data from the hydrothermal JADE field in the Okinawa back-arc trough. *Mineralium Deposita* **1997**, *32*, 70-78.
8. Halbach, P.N., Ko-Ichi ; Wahsner, M. ; Lange, J. ; Sakai, H. ; Käselitz, L. ; Hansen, R. -D. ; Yamano, M. ; Post, J. ; Prause, B. ; Seifert, R. ; Michaelis, W. ; Teichmann, F. ; Kinoshita, M. ; Märten, A. ; Ishibashi, J. ; Czerwinski, S. ; Blum, N. Probable modern analogue of Kuroko-type massive sulphide deposits in the Okinawa Trough back-arc basin. *Nature* **1989**, *338*, 496-499.
9. Halbach, P.; B. Pracejus Geology and Mineralogy of Massive Sulfide Ores from the Central Okinawa Trough, Japan. *Economic Geology and the Bulletin of the Society of Economic Geologists* **1993**, *88*, 2210-2225.
10. Marumo, K.; K.H. Hattori Seafloor hydrothermal clay alteration at Jade in the back-arc Okinawa Trough: Mineralogy, geochemistry and isotope characteristics. *Geochimica Et Cosmochimica Acta* **1999**, *63*, 2785-2804.
11. Luders, V.; B. Pracejus; P. Halbach Fluid inclusion and sulfur isotope studies in probable modem analogue Kuroko-type ores from the JADE hydrothermal field (Central Okinawa Trough, Japan). *Chemical Geology* **2001**, *173*, 45-58.
12. Zeng, Z.G.; X.Y. Wang; C.T.A. Chen; H.Y. Qi Understanding the Compositional Variability of the Major Components of Hydrothermal Plumes in the Okinawa Trough. *Geofluids* **2018**,
13. Zeng, Z.G.; Y. Ma; X.Y. Wang; C.T.A. Chen; X.B. Yin; S.P. Zhang; J.L. Zhang; W. Jiang Elemental compositions of crab and snail shells from the Kueishantao hydrothermal field in the southwestern Okinawa Trough. *Journal of Marine Systems* **2018**, *180*, 90-101.
14. Guo, K.; S.K. Zhai; Z.H. Yu; S.J. Wang; X. Zhang; X.Y. Wang Geochemical and Sr-Nd-Pb-Li isotopic characteristics of volcanic rocks from the Okinawa Trough: Implications for the influence of subduction components and the contamination of crustal materials. *Journal of Marine Systems* **2018**, *180*, 140-151.
15. Ishibashi, J.I.; F. Ikegami; T. Tsuji; T. Urabe Hydrothermal Activity in the Okinawa Trough Back-Arc Basin: Geological Background and Hydrothermal Mineralization. *Springer Japan* **2015**,
16. Zhang, Y.Y. Enrichment mechanism of gold and silver in hydrothermal sulfide from the okinawa trough. Zhejiang University.
17. Scott, S.D. Chemical Behavior of Sphalerite and Arsenopyrite in Hydrothermal and Metamorphic Environments. *Mineralogical Magazine* **1983**, *47*, 427-435.

18. Gallant, R.M.; K.L. Von Damm Geochemical controls on hydrothermal fluids from the Kairei and Edmond Vent Fields, 23 degrees-25 degrees S, Central Indian Ridge. *Geochemistry Geophysics Geosystems* **2006**, *7*,
19. Kristall, B.; D.S. Kelley; M.D. Hannington; J.R. Delaney Growth history of a diffusely venting sulfide structure from the Juan de Fuca Ridge: A petrological and geochemical study. *Geochemistry Geophysics Geosystems* **2006**, *7*,
20. Zeng, Z.G.; S. Niedermann; S. Chen; X.Y. Wang; Z.X. Li Noble gases in sulfide deposits of modern deep-sea hydrothermal systems: Implications for heat fluxes and hydrothermal fluid processes. *Chemical Geology* **2015**, *409*, 1-11.
21. Webber, A.P.; S. Roberts; B.J. Murton; R.A. Mills; M.R.S. Hodgkinson The formation of gold-rich seafloor sulfide deposits: Evidence from the Beebe hydrothermal vent field, Cayman Trough. *Geochemistry Geophysics Geosystems* **2017**, *18*, 2011-2027.
22. Letouzey, J.; M. Kimura The Okinawa Trough - Genesis of a Back-Arc Basin Developing Along a Continental-Margin. *Tectonophysics* **1986**, *125*, 209-230.
23. Sibuet, J.C.; B. Deffontaines; S.K. Hsu; N. Thareau; J.P. Le Formal; C.S. Liu; A. Party Okinawa trough backarc basin: Early tectonic and magmatic evolution. *Journal of Geophysical Research-Solid Earth* **1998**, *103*, 30245-30267.
24. Glasby, G.P.; K. Notsu Submarine hydrothermal mineralization in the Okinawa Trough, SW of Japan: an overview. *Ore Geology Reviews* **2003**, *23*, 299-339.
25. Shinjo, R.; S.L. Chung; Y. Kato; M. Kimura Geochemical and Sr-Nd isotopic characteristics of volcanic rocks from the Okinawa Trough and Ryukyu Arc: Implications for the evolution of a young, intracontinental back arc basin. *Journal of Geophysical Research-Solid Earth* **1999**, *104*, 10591-10608.
26. Kimura, M.; S. Uyeda; Y. Kato; T. Tanaka; M. Yamano; T. Gamo; H. Sakai; S. Kato; E. Izawa; T. Oomori Active Hydrothermal Mounds in the Okinawa Trough Backarc Basin, Japan. *Tectonophysics* **1988**, *145*, 319-324.
27. Zeng, Z.G.; Y.S. Qin; S.K. Zhai Helium, neon and argon isotope compositions of fluid inclusions in massive sulfides from the Jade hydrothermal field, the Oldnawa Trough. *Acta Oceanologica Sinica* **2004**, *23*, 655-661.
28. Zeng, Z.G.; Q.I. Haiyan; S. Chen; X.B. Yin; L.I. Zhaoxue Hydrothermal alteration of plagioclase microphenocrysts and glass in basalts from the East Pacific Rise near 13°N: An SEM-EDS study. *Science China(Earth Sciences)* **2014**, *000*, P.1427-1437.
29. Steadman, J.A.; R.R. Large; P.H. Olin; L.V. Danyushevsky; S. Meffre; D. Huston; A. Fabris; V. Lisitsin; T. Wells Pyrite trace element behavior in magmatic-hydrothermal environments: An LA-ICPMS imaging study. *Ore Geology Reviews* **2021**, *128*,
30. Barton, P.B.; P.M. Bethke Chalcopyrite Disease in Sphalerite - Pathology and Epidemiology. *American Mineralogist* **1987**, *72*, 451-467.
31. Melekestseva, I.Y.; G.A. Tret'yakov; P. Nimis; A.M. Yuminov; V.V. Maslennikov; S.P. Maslennikova; V.A. Kotlyarov; V.E. Beltenev; L.V. Danyushevsky; R. Large Barite-rich massive sulfides from the Semenov-1 hydrothermal field (Mid-Atlantic Ridge, 13 degrees 30.87 ' N): Evidence for phase separation and magmatic input. *Marine Geology* **2014**, *349*, 37-54.
32. Wohlgemuth-Ueberwasser, C.C.; F. Viljoen; S. Petersen; C. Vorster Distribution and solubility limits of trace elements in hydrothermal black smoker sulfides: An in-situ LA-ICP-MS study. *Geochimica Et Cosmochimica Acta* **2015**, *159*, 16-41.
33. Caye, R.; B. Cervelle; F. Cesbron; E. Oudin; P. Picot; F. Pillard Isocubanite, a New Definition of the Cubic Polymorph of Cubanite Cufe2s3. *Mineralogical Magazine* **1988**, *52*, 509-514.
34. Jun, Y., Mineralization of Polymetallic Sulfides on Ultra-slow Spreading Southwest Indian Ridge at 49.6°E, in The Institute of Oceanology, Chinese Academy of Sciences. 2010. p. 120.
35. Laskar, C.; E.F. Bazarkina; M.A. Kokh; J.L. Hazemann; R. Vuilleumier; E. Desmaele; G.S. Pokrovski Stability and structure of platinum sulfide complexes in hydrothermal fluids. *Geochimica Et Cosmochimica Acta* **2022**, *336*, 407-422.
36. Barnes, H.L.; H.L. Barnes, *Geochemistry of hydrothermal ore deposits*. 3rd ed. 1997, New York: Wiley. xx, 972 pages : illustrations, maps.
37. Zhang, H.Y.; Zhao, Q.Q.; Zhao, G.; Hong, J.X.; Liu, J.J.; Zhai, D.G. In situ LA-ICP-MS trace element analysis of pyrite and its application in study of Au deposit. *Mineral Deposits* **2022**, *41*, 18.
38. Zhou, T.F.; Zhang, L.J.; Yuan, F.; Fan, Y.; D.R. Cooke LA-ICP-MS in situ trace element analysis of pyrite from the Xinqiao Cu-Au-S Deposit in Tongling, Anhui, and its constraints on the ore genesis. *Earth Science Frontiers* **2010**, 14.
39. Cook, N.J.; C.L. Ciobanu; A. Pring; W. Skinner; M. Shimizu; L. Danyushevsky; B. Saini-Eidukat; F. Melcher Trace and minor elements in sphalerite: A LA-ICPMS study. *Geochimica Et Cosmochimica Acta* **2009**, *73*, 4761-4791.
40. Roman, N.; M. Reich; M. Leisen; D. Morata; F. Barra; A.P. Deditius Geochemical and micro-textural fingerprints of boiling in pyrite. *Geochimica Et Cosmochimica Acta* **2019**, *246*, 60-85.

41. Metz, S.; J.H. Trefry Chemical and mineralogical influences on concentrations of trace metals in hydrothermal fluids. *Geochimica Et Cosmochimica Acta* **2000**, *64*, 2267-2279.
42. Wang, Y.J.; X.Q. Han; S. Petersen; M. Frische; Z.Y. Qiu; H.M. Li; H.L. Li; Z.C. Wu; R.Y. Cui Mineralogy and trace element geochemistry of sulfide minerals from the Wocan Hydrothermal Field on the slow-spreading Carlsberg Ridge, Indian Ocean. *Ore Geology Reviews* **2017**, *84*, 1-19.
43. Huston, D.L.; S.H. Sie; G.F. Suter; D.R. Cooke; R.A. Both Trace-Elements in Sulfide Minerals from Eastern Australian Volcanic-Hosted Massive Sulfide Deposits .1. Proton Microprobe Analyses of Pyrite, Chalcopyrite, and Sphalerite, And .2. Selenium Levels in Pyrite - Comparison with Delta-S-34 Values and Implications for the Source of Sulfur in Volcanogenic Hydrothermal Systems. *Economic Geology and the Bulletin of the Society of Economic Geologists* **1995**, *90*, 1167-1196.
44. Ballantyne, J.M.; J.N. Moore Arsenic Geochemistry in Geothermal Systems. *Geochimica Et Cosmochimica Acta* **1988**, *52*, 475-483.
45. Maslennikov, V.V.; S.P. Maslennikova; R.R. Large; L.V. Danyushevsky Study of Trace Element Zonation in Vent Chimneys from the Silurian Yaman-Kasy Volcanic-Hosted Massive Sulfide Deposit (Southern Urals, Russia) Using Laser Ablation-Inductively Coupled Plasma Mass Spectrometry (LA-ICPMS). *Economic Geology* **2009**, *104*, 1111-1141.
46. Herzig, P.M.; M.D. Hannington Polymetallic massive sulfides at the modern seafloor - A review. *Ore Geology Reviews* **1995**, *10*, 95-115.
47. Reich, M.; A. Deditius; S. Chryssoulis; J.W. Li; C.Q. Ma; M.A. Parada; F. Barra; F. Mittermayr Pyrite as a record of hydrothermal fluid evolution in a porphyry copper system: A SIMS/EMPA trace element study. *Geochimica Et Cosmochimica Acta* **2013**, *104*, 42-62.
48. Vaughan, D.J.; K.M. Rosso Chemical bonding in sulfide minerals. *Sulfide Mineralolgy and Geochemistry* **2006**, *61*, 231-264.
49. Di Benedetto, F.; G.P. Bernardini; P. Costagliola; D. Plant; D.J. Vaughan Compositional zoning in sphalerite crystals. *American Mineralogist* **2005**, *90*, 1384-1392.
50. Frenzel, M.; T. Hirsch; J. Gutzmer Gallium, germanium, indium, and other trace and minor elements in sphalerite as a function of deposit type - A meta-analysis. *Ore Geology Reviews* **2016**, *76*, 52-78.
51. Keith, M.; K.M. Haase; U. Schwarz-Schampera; R. Klemd; S. Petersen; W. Bach Effects of temperature, sulfur, and oxygen fugacity on the composition of sphalerite from submarine hydrothermal vents. *Geology* **2014**, *42*, 699-702.
52. Yund, R.A.; H.T. Hall Hexagonal and Monoclinic Pyrrhotites. *Economic Geology* **1969**, *64*, 420-&.
53. Sauter, D.; H. Sloan; M. Cannat; J. Goff; P. Patriat; M. Schaming; W.R. Roest From slow to ultra-slow: How does spreading rate affect seafloor roughness and crustal thickness? *Geology* **2011**, *39*, 911-914.
54. Dahlem Workshop on, E.; S. Msss Transfer in Marine Hydrothermal; P. Halbach; V. Tunnicliffe; J.R. Hein, *Energy and mass transfer in marine hydrothermal systems*. Dahlem workshop report 89. 2003, Berlin, Germany: Dahlem University Press. xiv, 365 pages : illustrations.
55. Smith, R.N.; D.L. Huston Distribution and Association of Selected Trace-Elements at the Rosebery Deposit, Tasmania. *Economic Geology and the Bulletin of the Society of Economic Geologists* **1992**, *87*, 706-719.
56. Nesbitt, H.W.; L.J. Muir; A.R. Pratt Oxidation of Arsenopyrite by Air and Air-Saturated, Distilled Water, and Implications for Mechanism of Oxidation. *Geochimica Et Cosmochimica Acta* **1995**, *59*, 1773-1786.
57. Sugaki, A.; A. Kitakaze; S. Kojima Bulk Compositions of Intimate Intergrowths of Chalcopyrite and Sphalerite and Their Genetic-Implications. *Mineralium Deposita* **1987**, *22*, 26-32.
58. Todd, E.C.; D.M. Sherman; J.A. Purton Surface oxidation of chalcopyrite (CuFeS2) under ambient atmospheric and aqueous (pH 2-10) conditions: Cu, Fe L- and OK-edge X-ray spectroscopy. *Geochimica Et Cosmochimica Acta* **2003**, *67*, 2137-2146.
59. Mikhlin, Y.; Y. Tomashevich; V. Tauson; D. Vyalikh; S. Molodtsov; R. Szargan A comparative X-ray absorption near-edge structure study of bornite, Cu5FeS4, and chalcopyrite, CuFeS2. *Journal of Electron Spectroscopy and Related Phenomena* **2005**, *142*, 83-88.
60. Pearce, C.I.; R.A.D. Pattrick; D.J. Vaughan; C.M.B. Henderson; G. van der Laan Copper oxidation state in chalcopyrite: Mixed Cu d(9) and d(10) characteristics. *Geochimica Et Cosmochimica Acta* **2006**, *70*, 4635-4642.
61. George, L.L.; N.J. Cook; B.B.P. Crowe; C.L. Ciobanu Trace elements in hydrothermal chalcopyrite. *Mineralogical Magazine* **2018**, *82*, 59-88.
62. Ren, Y.Q.; C.C. Wohlgemuth-Ueberwasser; F. Huang; X.F. Shi; B. Li; M. Oelze; A. Schreiber; R. Wirth Distribution of trace elements in sulfides from Deyin hydrothermal field, Mid-Atlantic Ridge - Implications for its mineralizing processes. *Ore Geology Reviews* **2021**, *128*,
63. Keith, M.; F. Hackel; K.M. Haase; U. Schwarz-Schampera; R. Klemd Trace element systematics of pyrite from submarine hydrothermal vents. *Ore Geology Reviews* **2016**, *72*, 728-745.
64. Janecky, D.R.; W.E. Seyfried Formation of Massive Sulfide Deposits on Oceanic Ridge Crests - Incremental Reaction Models for Mixing between Hydrothermal Solutions and Seawater. *Geochimica Et Cosmochimica Acta* **1984**, *48*, 2723-2738.

65. Ruaya, J.R.; T.M. Seward The Stability of Chlorozinc(Ii) Complexes in Hydrothermal Solutions up to 350-Degrees-C. *Geochimica Et Cosmochimica Acta* **1986**, *50*, 651-661.
66. Crerar, D.A.; H.L. Barnes Ore Solution Chemistry .5. Solubilities of Chalcopyrite and Chalcocite Assemblages in Hydrothermal Solution at 200degrees to 350degreesc. *Economic Geology* **1976**, *71*, 772-794.
67. Seyfried, W.E.; K. Ding Phase equilibria in subseafloor hydrothermal systems: A Review of the role of Redox, temperature, pH and dissolved Cl on the chemistry of hot spring fluids at mid-ocean ridge. *AGU* **1995**,
68. Koski, R.A.; D.A. Clague; E. Oudin Mineralogy and Chemistry of Massive Sulfide Deposits from the Juan-De-Fuca Ridge. *Geological Society of America Bulletin* **1984**, *95*, 930-945.